JOURNAL OF AIRCRAFT
Vol. 46, No. 5, September–October 2009

Aerothermoacoustic Response of Shape Memory Alloy Hybrid Composite Panels

Hesham Hamed Ibrahim*
Hanyang University, Seoul 133-791, Republic of Korea
Mohammad Tawfik†
Emirates Aviation College, Dubai 53044, United Arab Emirates
Hani Mohammed Negm‡
Cairo University, Cairo 12613, Egypt
and
Hong Hee Yoo§
Hanyang University, Seoul 133-791, Republic of Korea

DOI: 10.2514/1.39214

Supersonic nonlinear vibrations of a traditional composite panel impregnated with prestrained shape memory alloy fibers and subjected to combined aerodynamic, thermal, and random acoustic loads are investigated. A nonlinear finite element model is developed using the first-order shear-deformable plate theory, von Kármán strain-displacement relations, and the principle of virtual work. The aerodynamic pressure is modeled using the quasi-steady first-order piston theory. Thermal load is assumed to be steady-state constant temperature distribution, and the acoustic excitation is considered to be a white-Gaussian random pressure with zero mean and uniform magnitude over the panel surface. Nonlinear temperature-dependence of material properties is considered in the formulation. The dynamic nonlinear equations of motion are transformed to modal coordinates to reduce the computational efforts. The Newton–Raphson iteration method is employed to obtain the dynamic response at each time step of the Newmark numerical integration scheme. Finally, the nonlinear response of a shape memory alloy hybrid composite panel is presented, illustrating the effect of shape memory alloy fiber embeddings, aerodynamic pressure, sound pressure level, and temperature rise on the panel response.

I. Introduction

THIN plates are a commonly used form of structural components, especially in aerospace vehicles, such as high-speed aircraft, rockets, and spacecraft, which are subjected to aerodynamic loads, thermal loads due to aerodynamic and/or solar radiation heating, and random acoustic loads due to engine and/or aerodynamic transonic noise. This results in temperature and pressure distributions over the panel surface. The presence of these thermal and pressure fields results in a flutter motion at a lower aerodynamic pressure, or a larger flutter limit-cycle amplitude at the same aerodynamic pressure. In addition, a high-temperature rise may cause large thermal deflections (thermal buckling) of the skin panels, which could affect flutter response. Accordingly, it is important to consider the interactive effect of aerodynamic, thermal, and random acoustic loads.

Panel flutter is a phenomenon that is usually accompanied by temperature elevation on the outer skin of high-speed air vehicles. Panel flutter is a self-excited oscillation of a plate or shell in supersonic flow. Because of aerodynamic pressure forces on the panel, two eigenmodes of the structure merge and lead to this dynamic instability. Panel flutter differs from wing flutter only in that the aerodynamic force resulting from the air flow acts only on one side of the panel. Most flutter analyses can be placed in one of four categories based on the structural and aerodynamic theories employed: 1) linear structural theory; quasi-steady aerodynamic theory, 2) linear structural theory; full linearized (inviscid, potential) aerodynamic theory, 3) nonlinear structural theory; quasi-steady aerodynamic theory, or 4) nonlinear structural theory; linearized (inviscid, potential) aerodynamic theory. Analyses of the first type have two major weaknesses: a) it does not account for structural nonlinearities, hence it can only determine the flutter boundary and can give no information about the flutter amplitudes, and b) the use of quasi-steady aerodynamics neglects the three-dimensionality and unsteadiness of the flow, hence it cannot be used in the transonic region where the flutter is most likely to occur. Analyses of the second type are intended to remedy weakness b, but this type still has weakness a. The third type remedies weakness a, but still possesses weakness b. The fourth type remedies both weakness a and b [1]. Mei et al. [2] provided a review on the various analytical methods and experimental results of supersonic and hypersonic panel flutter. An eigenvalue solution was developed by Dixon and Mei [3] for the nonlinear flutter analysis of thin composite panels using a linearized updated mode with nonlinear time function approximation. Xue and Mei [4] presented an incremental finite element frequency-domain solution for the nonlinear flutter response of thin isotropic panels under combined thermal and aerodynamic loads. Liaw [5] studied the nonlinear supersonic flutter of thin laminated composite plate structures subjected to thermal loads. Abdel-Motagaly et al. [6] investigated the effect of flow direction on the flutter limit-cycle amplitude of thick composite panels.

The surface panels of advanced high-speed aircraft and spacecraft may exhibit large random vibration under high acoustic loads, and may possibly experience both random vibration and aerodynamic flutter at elevated temperatures. Both of these effects are nonlinear in nature, and their combined response can lead to difficulties in the prediction fatigue life. A literature review on the nonlinear response and sonic fatigue of surface panels was presented by Vaicaitis [7].

Received 19 June 2008; revision received 4 June 2009; accepted for publication 4 June 2009.

*Assistant Professor, Space Division; currently National Authority for Remote Sensing and Space Sciences, Cairo 11769, Egypt; hesham.ibrahim@narss.sci.eg.

†Assistant Professor, Engineering Department; mohammad.tawfik@gmail.com.

‡Professor, Aerospace Engineering Department; hmnegm_cu@hotmail.com.

§Professor, Department of Mechanical Engineering; hhyoo@hanyang.ac.kr.

Experiments were performed to study thermally loaded panels under random excitation by Istenes et al. [8], Ng and Clevenson [9], and Murphy et al. [10], where a snap-through phenomenon and frequency shifting due to nonlinear large-amplitude vibration were observed. Kavallieratos and Vaicaitis [11] studied the nonlinear response of composite skin panels of high-speed aircraft. Locke [12] investigated the large deflection random vibration of a thermally buckled thin isotropic plate, using the method of equivalent linearization, while assuming temperature-independent material properties. The finite element numerical integration was adopted by Abdel-Motagaly et al. [13] to study the nonlinear panel response under combined aerodynamic and acoustic loads. They did not take into account the effect of elevated temperatures on the panel response. Dhainaut et al. [14] presented a finite element formulation for the prediction of nonlinear random response of thin isotropic and composite panels subjected to the simultaneous action of high acoustic loads and elevated temperatures.

Shape memory alloys (SMAs) refer to a group of materials which have the ability to return to a predetermined shape when heated. The shape memory effect is caused by a temperature-dependent crystalline structure. When an SMA is below its phase-transformation temperature, it possesses a low yield strength crystallography referred to as martensite. While in this state, the material can be deformed into other shapes with relatively little force. The new shape is retained provided the material is kept below its transformation temperature. When heated above this temperature, the material reverts to its parent structure known as austenite, causing it to return to its original shape. During the shape recovery process, a large tensile recovery stress occurs if the SMA is restrained. Both the recovery stresses and Young's modulus of SMA exhibit highly nonlinear temperature-dependent properties. Birman [15] presented a comprehensive review on the literature concerning SMA up to 1997. Jia and Rogers [16] formulated a mechanical model for composite plates with embedded shape memory alloy fibers using the micromechanical behavior of the highly nonlinear shape memory alloy. Tawfik et al. [17] proposed a novel concept in enhancing the thermal buckling and aeroelastic behavior of plates through embedding SMA fibers in it. Park et al. [18] adopted the incremental finite element procedure presented in [17] to study the effect of SMA fiber embeddings on the nonlinear vibration behavior of thick, thermally buckled composite plates. Gilat and Aboudi [19] derived micromechanically established constitutive equations for unidirectional composites with shape memory alloy fibers embedded in polymeric metallic matrices. These equations were subsequently employed to analyze the nonlinear behavior of infinitely wide composite plates that are subject to sudden application of thermal loading. Ibrahim et al. [20] developed a frequency-domain solution for predicting the critical aerodynamic pressures of shape memory alloy hybrid composite (SMAHC) panels at elevated temperatures. Guo et al. [21] investigated the large-amplitude nonlinear flutter of thin SMAHC panels with arbitrary supersonic yawed angle and elevated temperatures. Ibrahim et al. [22] presented a finite element formulation to investigate the nonlinear random response of thick composite plates impregnated with prestrained SMA fibers subject to thermal and random acoustic loads. However, to the best of authors' knowledge, the combined effect of aerodynamic, thermal, and acoustic loads on the supersonic nonlinear vibration behavior of SMAHC panels has not yet been accomplished in the literature. As the use of SMAHC panels is expected to increase, it is worth investigating the nonlinear response of such panels under combined aerodynamic, thermal, and random acoustic loads.

This paper is an extension of the work presented by Ibrahim et al. [22]. A time-domain solution is presented for the supersonic nonlinear vibration behavior of clamped SMAHC panels under combined aerodynamic, thermal, and random acoustic loads. A nonlinear finite element model is provided based on the first-order shear plate theory with von Kármán geometric nonlinearity and the principle of virtual work. The first-order piston theory is adopted to model aerodynamic pressures induced by supersonic airflows. The thermal load is assumed to be steady-state constant temperature distribution, and the acoustic excitation is considered to be a stationary white-Gaussian random pressure with zero mean and uniform magnitude over the plate surface. Nonlinear temperature-dependence of material properties is considered in the formulation. The governing equations are transformed to modal coordinates to reduce the computational efforts. The Newton–Raphson iteration method is employed to obtain the dynamic response at each time step of the Newmark numerical integration scheme. Finally, numerical results are provided to study the effects of SMA fiber embeddings, aerodynamic pressure, temperature rise, and random acoustic load on the panel response.

II. Finite Element Formulation

A. Nonlinear Strain-Displacement Relations

The nodal degrees-of-freedom vector of a nine-noded rectangular element, shown in Fig. 1, can be written as

$$\{\theta\} = \{\{w_b\}, \{\phi_x, \phi_y\}, \{u, v\}\}^T = \begin{Bmatrix} \{w_b\} \\ \{w_\phi\} \\ \{w_m\} \end{Bmatrix} = \begin{Bmatrix} \{w_B\} \\ \{w_m\} \end{Bmatrix} \tag{1}$$

where w_b is the transverse displacement of the middle plane, ϕ_x and ϕ_y are rotations of the transverse normal about the x and y axes, respectively, and u and v are the membrane displacements in the x and y directions, respectively. The displacement-nodal displacement relations can be presented in terms of interpolation function matrices, $[N_w]$, $[N_{\phi x}]$, $[N_{\phi y}]$, $[N_u]$, and $[N_v]$ as

$$\begin{aligned} w &= [H_w][T_b]^{-1}\{w_b\} = [N_w]\{w_b\} \\ \phi_x &= \lfloor H_{\phi x} \rfloor [T_\phi]^{-1}\{w_\phi\} = [N_{\phi x}]\{w_\phi\} \\ \phi_y &= \lfloor H_{\phi y} \rfloor [T_\phi]^{-1}\{w_\phi\} = [N_{\phi y}]\{w_\phi\} \\ u &= [H_u][T_m]^{-1}\{w_m\} = [N_u]\{w_m\} \\ \text{and} \quad v &= [H_v][T_m]^{-1}\{w_m\} = [N_v]\{w_m\} \end{aligned} \tag{2}$$

where

$$\begin{aligned} [H_w] &= \lfloor 1 \;\; x \;\; y \;\; xy \;\; x^2 \;\; y^2 \;\; x^2y \;\; xy^2 \;\; x^2y^2 \rfloor \\ [H_{\phi x}] &= \lfloor 1 \;\; x \;\; y \;\; xy \;\; x^2 \;\; y^2 \;\; x^2y \;\; xy^2 \;\; x^2y^2 \;\; 0 \;\; 0 \;\; 0 \;\; 0 \;\; 0 \;\; 0 \;\; 0 \;\; 0 \rfloor \\ [H_{\phi y}] &= \lfloor 0 \;\; 0 \;\; 0 \;\; 0 \;\; 0 \;\; 0 \;\; 0 \;\; 0 \;\; 0 \;\; 1 \;\; x \;\; y \;\; xy \;\; x^2 \;\; y^2 \;\; x^2y \;\; xy^2 \;\; x^2y^2 \rfloor \\ [H_u] &= \lfloor 1 \;\; x \;\; y \;\; xy \;\; x^2 \;\; y^2 \;\; x^2y \;\; xy^2 \;\; x^2y^2 \;\; 0 \;\; 0 \;\; 0 \;\; 0 \;\; 0 \;\; 0 \;\; 0 \;\; 0 \rfloor \\ [H_v] &= \lfloor 0 \;\; 0 \;\; 0 \;\; 0 \;\; 0 \;\; 0 \;\; 0 \;\; 0 \;\; 0 \;\; 1 \;\; x \;\; y \;\; xy \;\; x^2 \;\; y^2 \;\; x^2y \;\; xy^2 \;\; x^2y^2 \rfloor \end{aligned}$$

In-plane strains and curvatures, based on von Kármán's moderately large deflection and first-order shear-deformable plate theory, are given by [23]

$$\begin{Bmatrix} \varepsilon_x \\ \varepsilon_y \\ \gamma_{xy} \end{Bmatrix} = \begin{Bmatrix} \frac{\partial u}{\partial x} \\ \frac{\partial v}{\partial y} \\ \frac{\partial u}{\partial y} + \frac{\partial v}{\partial x} \end{Bmatrix} + \begin{Bmatrix} \frac{1}{2}\left(\frac{\partial w}{\partial x}\right)^2 \\ \frac{1}{2}\left(\frac{\partial w}{\partial y}\right)^2 \\ \frac{\partial w}{\partial x}\frac{\partial w}{\partial y} \end{Bmatrix} + z \begin{Bmatrix} \frac{\partial \phi_y}{\partial x} \\ \frac{\partial \phi_x}{\partial y} \\ \frac{\partial \phi_y}{\partial y} + \frac{\partial \phi_x}{\partial x} \end{Bmatrix} = \{\varepsilon_{\text{lin}}\}$$

$$+ \{\varepsilon_\theta\} + z\{\kappa\} \tag{3}$$

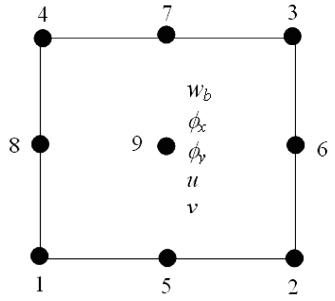

Fig. 1 Nodal degrees of freedom of a nine-noded rectangular element.

where $\{\varepsilon_{\text{lin}}\}$, $\{\varepsilon_\theta\}$, and $z\{\kappa\}$ are the membrane linear strain vector, the membrane nonlinear strain vector, and the bending strain vector, respectively, whereas the transverse shear strain vector can be expressed as [23]

$$\begin{Bmatrix}\gamma_{yz}\\ \gamma_{xz}\end{Bmatrix} = \begin{Bmatrix}\phi_x\\ \phi_y\end{Bmatrix} + \begin{Bmatrix}\frac{\partial w}{\partial y}\\ \frac{\partial w}{\partial x}\end{Bmatrix} \tag{4}$$

B. Constitutive Equations

For the kth composite lamina impregnated with SMA fibers, the stress–strain relations can be expressed as [22]

$$\{\sigma^k\} = \begin{Bmatrix}\sigma_x^k\\ \sigma_y^k\\ \tau_{xy}^k\end{Bmatrix} = [\bar{Q}^k(T)]\{\varepsilon\} + V_s^k\{\sigma_r^k(T)\} - V_m^k\int_{T_{\text{ref}}}^{T}[\bar{Q}_m^k(\tau)]\{\alpha_m^k(\tau)\}\,\mathrm{d}\tau \tag{5}$$

$$\{\tau^k\} = \begin{Bmatrix}\tau_{yz}^k\\ \tau_{xz}^k\end{Bmatrix} = \begin{bmatrix}\bar{Q}_{44}(T) & \bar{Q}_{45}(T)\\ \bar{Q}_{45}(T) & \bar{Q}_{55}(T)\end{bmatrix}\begin{Bmatrix}\gamma_{yz}\\ \gamma_{xz}\end{Bmatrix} \tag{6}$$

where subscripts m, s mean that the corresponding quantity or matrix is related to the composite matrix and the SMA fibers, respectively. The in-plane stress vector, the SMA recovery stress vector at a given temperature T, and the transverse shear stress vector are given by $\{\sigma\}$, $\{\sigma_r\}$, and $\{\tau\}$, respectively. V_m and V_s are the volume fractions of the composite matrix and SMA fibers, respectively. In addition, $\{\alpha_m\}$, $[\bar{Q}]$, and $[\bar{Q}_m]$ are the thermal expansion coefficient vector of the composite matrix, the transformed reduced stiffness matrix of the SMA embedded lamina, and the transformed reduced stiffness matrix of the composite matrix, respectively. Note that the SMA fiber is embedded in the same direction of the composite matrix fibers, and assumed uniformly distributed within each layer. Integrating Eqs. (4) and (5) over the plate thickness h, the constitutive equation is obtained as

$$\begin{Bmatrix}\{N\}\\ \{M\}\end{Bmatrix} = \begin{bmatrix}[A] & [B]\\ [B] & [D]\end{bmatrix}\begin{Bmatrix}\{\varepsilon_{\text{lin}}\} + \{\varepsilon_\theta\}\\ \{\kappa\}\end{Bmatrix} - \begin{Bmatrix}\{N^T\}\\ \{M^T\}\end{Bmatrix} + \begin{Bmatrix}\{N_r\}\\ \{M_r\}\end{Bmatrix} \tag{7}$$

$$\{R\} = \begin{Bmatrix}R_{yz}\\ R_{xz}\end{Bmatrix} = \begin{bmatrix}A_{44} & A_{45}\\ A_{45} & A_{55}\end{bmatrix}\begin{Bmatrix}\gamma_{yz}\\ \gamma_{xz}\end{Bmatrix} = [A_s]\{\gamma\} \tag{8}$$

where

$$\begin{Bmatrix}\{N^T\}\\ \{M^T\}\end{Bmatrix} = V_m\int_{-h/2}^{h/2}\left[\left(\int_{T_{\text{ref}}}^{T}[Q_m(\tau)]\{\alpha_m(\tau)\}\,\mathrm{d}\tau\right)\right]\begin{Bmatrix}1\\ z\end{Bmatrix}\mathrm{d}z$$

$$\begin{Bmatrix}\{N_r\}\\ \{M_r\}\end{Bmatrix} = V_s\int_{-h/2}^{h/2}\{\sigma_r\}\begin{Bmatrix}1\\ z\end{Bmatrix}\mathrm{d}z$$

C. Aerodynamic Loading

The aerodynamic pressure caused by a supersonic airflow will be approximated by the first-order quasi-steady piston theory [17], which is valid for $\sqrt{2} < M_\infty$ and shows good accuracy in the range of $\sqrt{2} < M_\infty < 5$. The aerodynamic pressure using the first-order piston theory is expressed as

$$P_a = -\left(\frac{g_a}{\omega_0}\frac{D_{110}}{a^4}\frac{\partial w}{\partial t} + \lambda\frac{D_{110}}{a^3}\frac{\partial w}{\partial x}\right) \tag{9}$$

with

$$g_a = \sqrt{\lambda C_a}, \qquad C_a = \frac{(M_\infty^2-2)^2}{(M_\infty^2-1)^2}\frac{\rho_a a}{\rho h\beta}, \qquad \lambda = \frac{2qa^3}{\beta D_{110}}$$

$$q = \frac{\rho_a v^2}{2}, \qquad \beta = \sqrt{M_\infty^2-1}, \quad \text{and} \quad \omega_o = \left(\frac{D_{110}}{\rho h a^4}\right)^{\frac{1}{2}}$$

where P_a is the aerodynamic pressure loading, v is the airflow velocity on one side of the panel, M_∞ is the Mach number, q is the dynamic pressure, ρ and ρ_a are the panel and air mass densities, g_a is the nondimensional aerodynamic damping, C_a is the aerodynamic damping coefficient, λ is the nondimensional dynamic pressure, D_{110} is the first entry in the flexural stiffness matrix D (1, 1) when all the fibers of the composite layers are aligned in the airflow x direction, and a is the streamwise panel length.

D. Acoustic Load Simulation

The acoustic excitation is assumed as a stationary white-Gaussian random pressure with zero mean and uniform magnitude over the panel surface. Noting that, for the finite element time-domain integration method presented in this study, there is no limitation on the random input excitation. It can be stationary or nonstationary and Gaussian or non-Gaussian, as long as a time history for the random excitation is available. The cross-spectrum density S_p of a truncated white-Gaussian pressure uniformly distributed over the panel surface can be given as [14]

$$S_p = \begin{cases} S_o = p_o^2 10^{\text{SPL}/10}, & 0 \le f \le f_u\\ 0, & f < 0 \text{ or } f > f_u\end{cases} \tag{10}$$

where S_o is a constant, p_o is a reference pressure, $p_o = 20\ \mu$ Pa, SPL is sound pressure level in decibels, and f_u is the upper cutoff frequency in hertz. Using MATLAB, the Gaussian random pressure $p(t)$ with zero mean and power PW is expressed as

$$p(t) = \text{sqrt}(PW)\cdot\text{randn}([n, 1]) \tag{11}$$

where randn is the Gaussian random number generation function, and n is the amount of numbers need to be generated. For numerical integration, it is equal to the time duration divided by the time step. The power can be calculated from spectrum density S_o and upper cutoff frequency f_u as

$$PW = S_o\cdot f_u \tag{12}$$

The cutoff frequency should be selected so that it does not only cover the highest natural frequency in the simulation, but also considers the frequency shifting effect due to the nonlinear large-amplitude vibration. General speaking, it should be selected as at least twice the highest linear frequency of the modes included in the simulation.

E. Governing Equations

By using the principle of virtual work and Eqs. (3), (4), (7), and (8), the nonlinear governing equation can be derived as follows:

$$\delta W = \delta W_{\text{int}} - \delta W_{\text{ext}} = 0 \tag{13}$$

The internal virtual work δW_{int} can be stated as

$$\begin{aligned}\delta W_{\text{int}} &= \int_A(\{\delta(\varepsilon_{\text{lin}}+\varepsilon_\theta)\}^T\{N\} + \{\delta\kappa\}^T\{M\} + \{\delta\gamma\}^T\{R\})\,\mathrm{d}A\\ &= \{\delta\theta\}^T([k]-[k_T]+[k_r]+\tfrac{1}{2}[n1]+\tfrac{1}{3}[n2])\{\theta\}\\ &\quad -\{\delta\theta\}^T(\{p_T\}-\{p_r\})\end{aligned} \tag{14}$$

where $[k]$, $[k_T]$, and $[k_r]$ are the linear, thermal, and recovery stress stiffness matrices, and $[n1]$ and $[n2]$ are the first- and second-order nonlinear stiffness matrices, respectively. In addition, $\{p_T\}$ and $\{p_r\}$ are the thermal and recovery load vectors, respectively. On the other hand, the external virtual work δW_{ext} can be stated as [13]

$$\delta W_{\text{ext}} = \int_A [-I_o(\{\delta u\}^T\{\ddot{u}\} + \{\delta v\}^T\{\ddot{v}\} + \{\delta w\}^T\{\ddot{w}_b\}) - I_2(\{\delta\phi_x\}^T\{\ddot{\phi}_x\} + \{\delta\phi_y\}^T\{\ddot{\phi}_y\}) + \{\delta w_b\}^T P_a + \{\delta w_b\}^T p(t)]\,dA = -\{\delta\theta\}^T[m]\{\ddot{\theta}\} - \{\delta\theta\}^T[g]\{\dot{\theta}\} - \{\delta\theta\}^T\lambda[a_a]\{\theta\} + \{\delta\theta\}^T p(t) \tag{15}$$

where

$$(I_o, I_2) = \int_{-h/2}^{h/2} \rho(1, z^2)\,dz$$

with h denoting the plate thickness, $[m]$ as the mass matrix, $[g]$ as the aerodynamic damping matrix, $[a_a]$ as the aerodynamic influence matrix, and $p(t)$ as the acoustic load modeled as a white-Gaussian random pressure. By substituting Eqs. (14) and (15) into Eq. (13), the governing equations of motion can be written as follows:

$$\begin{bmatrix} M_B & 0 \\ 0 & 0 \end{bmatrix}\begin{Bmatrix} \ddot{W}_B \\ \ddot{W}_m \end{Bmatrix} + \begin{bmatrix} G_B & 0 \\ 0 & 0 \end{bmatrix}\begin{Bmatrix} \dot{W}_B \\ \dot{W}_m \end{Bmatrix} + \left(\lambda\begin{bmatrix} A_{aB} & 0 \\ 0 & 0 \end{bmatrix} + \begin{bmatrix} K_B & 0 \\ 0 & K_m \end{bmatrix} - \begin{bmatrix} K_{TB} & 0 \\ 0 & 0 \end{bmatrix} + \begin{bmatrix} K_{rB} & 0 \\ 0 & 0 \end{bmatrix} + \frac{1}{2}\begin{bmatrix} N1_{NmB} & N1_{Bm} \\ N1_{mB} & 0 \end{bmatrix} + \frac{1}{3}\begin{bmatrix} N2_B & 0 \\ 0 & 0 \end{bmatrix}\right)\begin{Bmatrix} W_B \\ W_m \end{Bmatrix} = \begin{Bmatrix} P_B(t) \\ 0 \end{Bmatrix} + \begin{Bmatrix} 0 \\ P_{mT} \end{Bmatrix} - \begin{Bmatrix} 0 \\ P_{mr} \end{Bmatrix} = \begin{Bmatrix} P_B \\ P_m \end{Bmatrix} \tag{16}$$

where subscripts a, B, m, T, and r stand for aerodynamic, bending, membrane, thermal, and recovery stress, respectively. Note that neglecting the in-plane inertia term in Eq. (16) will not bring significant error, because their natural frequencies are 2–3 orders of magnitude higher than those of bending [13].

III. Solution Procedures

In this section, a time-domain solution is presented for the nonlinear response of symmetrically laminated shape memory alloy hybrid composite plates. Separating the membrane and transverse displacement equations in Eq. (16) results in

$$[M_B]\{\ddot{W}_B\} + [G_B]\{\dot{W}_B\} + (\lambda[A_{aB}] + [K_B] - [K_{TB}] + [K_{rB}] + \tfrac{1}{2}[N1_{NmB}(\{W_m\})] + \tfrac{1}{3}[N2_B])\{W_B\} + \tfrac{1}{2}[N1_{Bm}]\{W_m\} = \{P_B\} \tag{17}$$

$$[K_m]\{W_m\} + \tfrac{1}{2}[N1_{mB}]\{W_B\} = \{P_m\} \tag{18}$$

From Eq. (18), the in-plane displacement vector $\{W_m\}$ can be expressed in terms of the bending displacement vector $\{W_B\}$ as

$$\{W_m\} = [K_m]^{-1}\{P_m\} - \tfrac{1}{2}[K_m]^{-1}[N1_{mB}]\{W_B\} = \{W_m\}_o - \{W_m\}_2 \tag{19}$$

where $\{W_m\}_o$ is a constant, and $\{W_m\}_2$ is quadratically dependent on $\{W_B\}$. Thus, the matrix $[N1_{NmB}(\{W_m\})]$ is evaluated by the algebraic sum of two components: $[N1_{NmB}(\{W_m\}_o)]$ and $[N1_{NmB}(\{W_m\}_2)]$, which are independent and quadratically dependent on $\{W_B\}$, respectively. Substituting Eq. (19) into Eq. (17), the system equations of motion can be stated as a function of $\{W_B\}$ as

$$[M_B]\{\ddot{W}_B\} + [G_B]\{\dot{W}_B\} + (\lambda[A_{aB}] + [K_B] - [K_{TB}] + [K_{rB}] + \tfrac{1}{2}[N1_{NmB}(\{W_m\})] + \tfrac{1}{3}[N2_B])\{W_B\} + \tfrac{1}{2}[N1_{Bm}]([K_m]^{-1}\{P_m\} - \tfrac{1}{2}[K_m]^{-1}[N1_{mB}]\{W_B\}) = \{P_B\} \tag{20}$$

It can be shown that [24]

$$\tfrac{1}{2}[N1_{Bm}]\{W_m\}_o = \tfrac{1}{2}[N1_{NmB}(\{W_m\}_o)]\{W_B\} \tag{21}$$

According to Eq. (21), the system equation of motions can be finally stated as

$$[M_B]\{\ddot{W}_B\} + [G_B]\{\dot{W}_B\} + (\lambda[A_{aB}] + [K_B] - [K_{TB}] + [K_{rB}] + [N1_{NmB}(\{W_m\}_o)])\{W_B\} + (\tfrac{1}{3}[N2_B] - \tfrac{1}{2}[N1_{NmB}(\{W_m\}_2)] - \tfrac{1}{4}[N1_{Bm}][K_m]^{-1}[N1_{mB}])\{W_B\} = \{P_B\} \tag{22}$$

Equation (22) can be numerically integrated in the structural nodal degrees of freedom. However, this approach turns to be computationally expensive. Therefore, an alternative and effective solution procedure is to transform Eq. (22) into modal coordinates using reduced system normal modes by expressing the system bending displacement $\{W_B\}$ as a linear combination of a finite number of normal mode shapes as

$$\{W_B\} \approx \sum_{r=1}^{n} Q_r\{\phi_r\} = [\Phi]\{Q\} \tag{23}$$

where the rth normal mode $\{\phi_r\}$ and the corresponding natural frequency ω_r are obtained from the linear vibration of the system as

$$\omega_r^2[M_B]\{\phi_r\} = ([K_B])\{\phi_r\} \tag{24}$$

Accordingly, all the matrices in Eq. (22) are transformed into modal coordinates and it can be written in modal coordinates as

$$[\bar{M}_B]\{\ddot{Q}\} + [\bar{G}_B]\{\dot{Q}\} + 2[\zeta_r f_r][\bar{M}_B]\{\dot{Q}\} + ([\bar{K}] + [\bar{K}_{qq}])\{Q\} = \{\bar{P}_B\} \tag{25}$$

where the modal mass, aerodynamic, and linear stiffness matrices are given by

$$([\bar{M}_B], [\bar{G}_B], [\bar{K}]) = [\Phi]^T([M_B], [G_B], [K_{\text{lin}}])[\Phi] \tag{26}$$

$$[K_{\text{lin}}] = \lambda[A_{aB}] + [K_B] - [K_{TB}] + [K_{rB}] + [N1_{NmB}(\{W_m\}_o)] \tag{27}$$

$$\{\bar{P}_B\} = [\Phi_B]^T\{P_B\} = [\Phi_B]^T\begin{Bmatrix} P_b(t) \\ 0 \end{Bmatrix} \tag{28}$$

The second-order nonlinear modal stiffness matrix is given by

$$[\bar{K}_{qq}] = [\Phi]^T\sum_{r=1}^{n}\sum_{s=1}^{n} Q_r Q_s(\tfrac{1}{3}[N2_B]^{(rs)} - \tfrac{1}{2}[N1_{NmB}(\{W_m\}_2)]^{(rs)} - \tfrac{1}{4}[N1_{Bm}]^{(r)}[K_m]^{-1}[N1_{mB}]^{(s)})[\Phi] \tag{29}$$

Note that a modal structural damping matrix $2\,[\zeta_r f_r]\,[M_B]$ has been added to Eq. (25) to account for the structural damping effect on the system [21]. The coefficient ζ_r is the modal damping ratio of the rth mode, whereas f_r is the rth natural frequency in hertz.

IV. Numerical Results and Discussions

The nonlinear vibration behavior of a SMAHC panel is investigated with four parameters in the study: SMA volume fraction V_s, temperature rise ΔT, sound pressure level SPL, and nondimensional dynamic pressure λ. The panel is modeled using an 8×8 mesh. A traditional clamped composite plate and a SMAHC plate with 10% volume fraction and 3% prestrain are studied and compared. All panel edges are assumed clamped. Typical values were chosen for the structural and aerodynamic damping coefficients. A proportional damping ratio of $\zeta_r f_r = \zeta_s f_s$ is used with a fundamental modal damping coefficient ζ_1 equal to 0.02. The aerodynamic damping coefficient C_a is set to 0.1. A uniform temperature elevation is applied to the plate, and the reference temperature is assumed to be 21°C. A Newmark implicit numerical integration scheme is used to

Table 1 Material properties of composite matrix and SMA fiber

Nitinol	Graphite-epoxy
See Figs. 1 and 2 for Young's modulus and recovery stresses	E1 $155\,(1-6.35\times10^{-4}T)$ GPa
	E2 $8.07\,(1-7.69\times10^{-4}T)$ GPa
G 25.6 GPa	G12 $4.55\,(1-1.09\times10^{-3}T)$ GPa
ρ 6450 Kg/m^3	ρ 1550 Kg/m^3
ν 0.3	ν 0.22
α 10.26×10^{-6}/°C	$\alpha1$ $-0.07\times10^{-6}(1-0.69\times10^{-3}T)$/°C
	$\alpha2$ $30.6\times10^{-6}(1+0.28\times10^{-4}T)$/°C

solve the system differential equations, and a Newton–Raphson iteration scheme is adopted to solve the nonlinear algebraic system of equations at each time step [25]. Modal transformation using nine normal modes was found giving a converged solution and thus used, noting that linear normal modes can efficiently express the panel nonlinear response in panels with all edges clamped [26]. The dimensions of the panel are $0.381\times0.305\times0.0013$ m with a stacking sequence $[0/-45/45/90]_s$. Table 1 presents the material properties of both the composite matrix and the SMA fibers [22], while the variation of the modulus of elasticity and recovery stress of a trained SMA fibers, made from nitinol, are presented in Figs. 2 and 3 [27]. The length of the simulated process is chosen to be 1 s in this study. The fundamental frequency of the composite panel selected for this study is about 109 Hz, and the fundamental period is 0.00917 s. Thus, the simulated process covers 109 natural periods of the panel. It has been shown in previous studies that, for a stationary response, reasonable statistical properties are obtained from a time history that contains more than 100 natural periods of the structure [28]. The linear frequency for the ninth mode (1, 5) is 1629 Hz, and so the cutoff frequency for this simulation is selected as 2000 Hz, which is large enough to cover the shifted frequency caused by nonlinear effects [14].

A. Validation of the Formulation

To validate the present formulation, the flutter limit-cycle oscillation amplitudes were calculated for an aluminum square panel

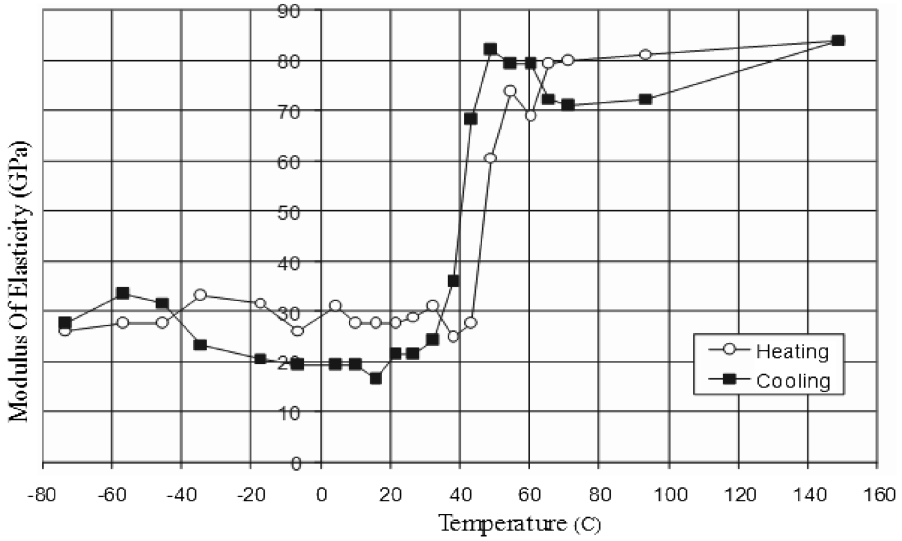

Fig. 2 Modulus of elasticity variation with temperature for a trained nitinol fiber.

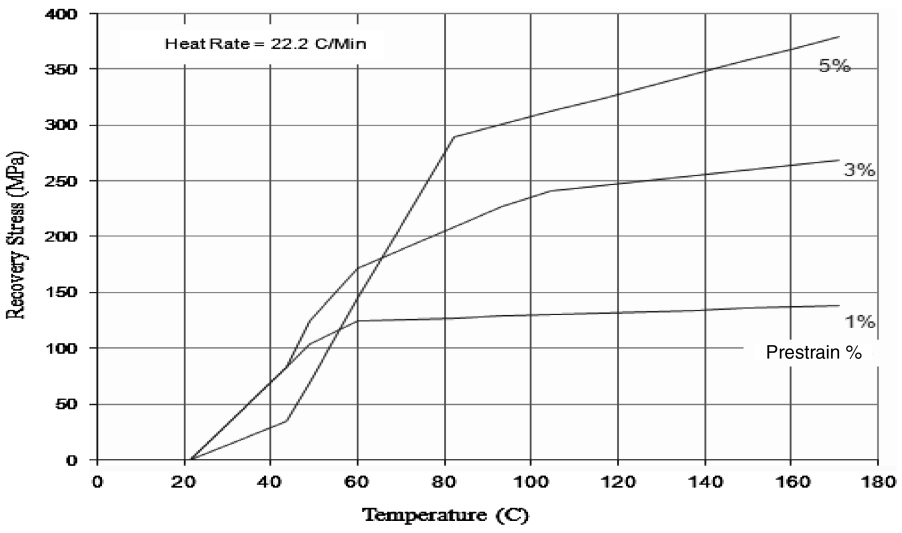

Fig. 3 Nitinol recovery stress as a function of both temperature and prestrain percentage.

at different values of the nondimensional dynamic pressure λ. The panel dimensions are $0.305 \times 0.305 \times 0.00127$ m with all edges simply supported. The aerodynamic damping coefficient C_a is set to 0.1. Nine normal modes were used with a time step for numerical integration equal to 1/10000 s. It is seen in Fig. 4 that the flutter limit-cycle amplitudes predicted using the current finite element model are in a good agreement with those of Dowell [29].

B. Nonlinear Vibration Behavior

To assess the sensitivity of the flutter behavior to boundary conditions, Fig. 5 illustrates the flutter oscillations of a panel at $\lambda = 700$ and having all edges simply supported or clamped. It is seen in the figure that the support condition has a noticeable effect on the flutter amplitudes, through having lower amplitudes in the case of clamped boundaries compared to the simply supported case. Moreover, no change has been depicted in the flutter type, because both panels show nearly harmonic oscillations. The effect of the aerodynamic damping on the flutter motion is investigated in Fig. 6. The flutter oscillations and phase plots for a simply supported composite panel at $\lambda = 700$, $Ca = 0$, 0.05, and 0.1, $\Delta T = 0°\text{C}$, and $\text{SPL} = 0$ dB are presented. In the absence of the aerodynamic damping, that is, $Ca = 0$, the panel is seen to experience chaotic flutter motion. By increasing the value of Ca up to 0.05, the panel

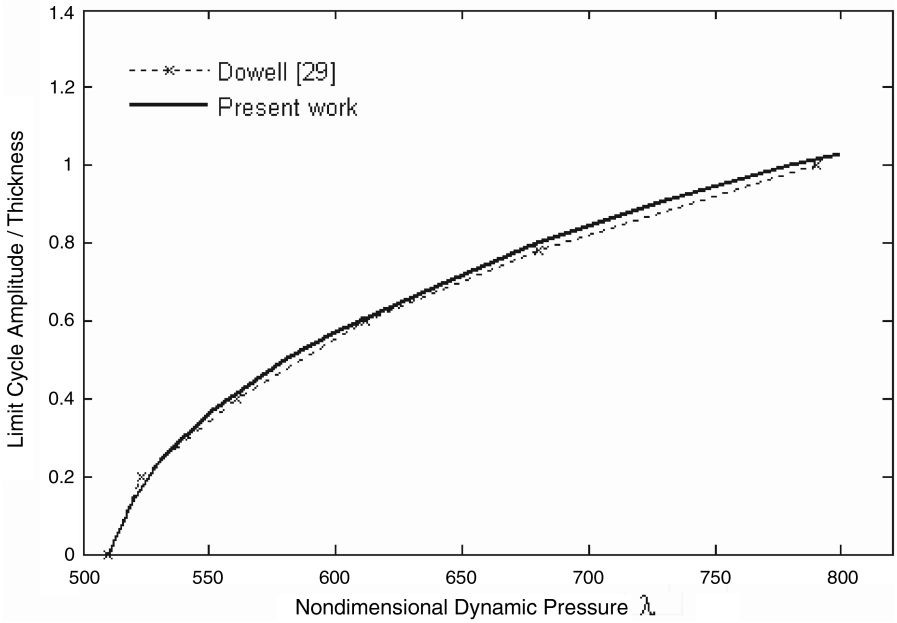

Fig. 4 Comparison of limit-cycle oscillation amplitudes between Dowell [29] and the current formulation for a simply supported aluminum square panel.

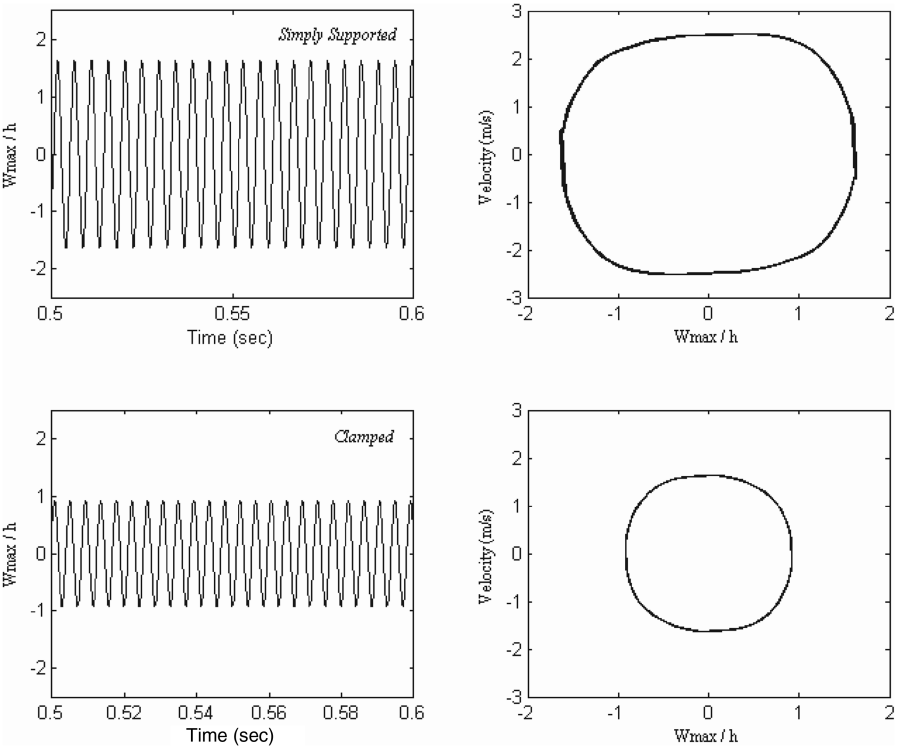

Fig. 5 Comparison of limit-cycle oscillation amplitudes between simply supported and clamped composite panels at $\lambda = 700$ and $Ca = 0.1$.

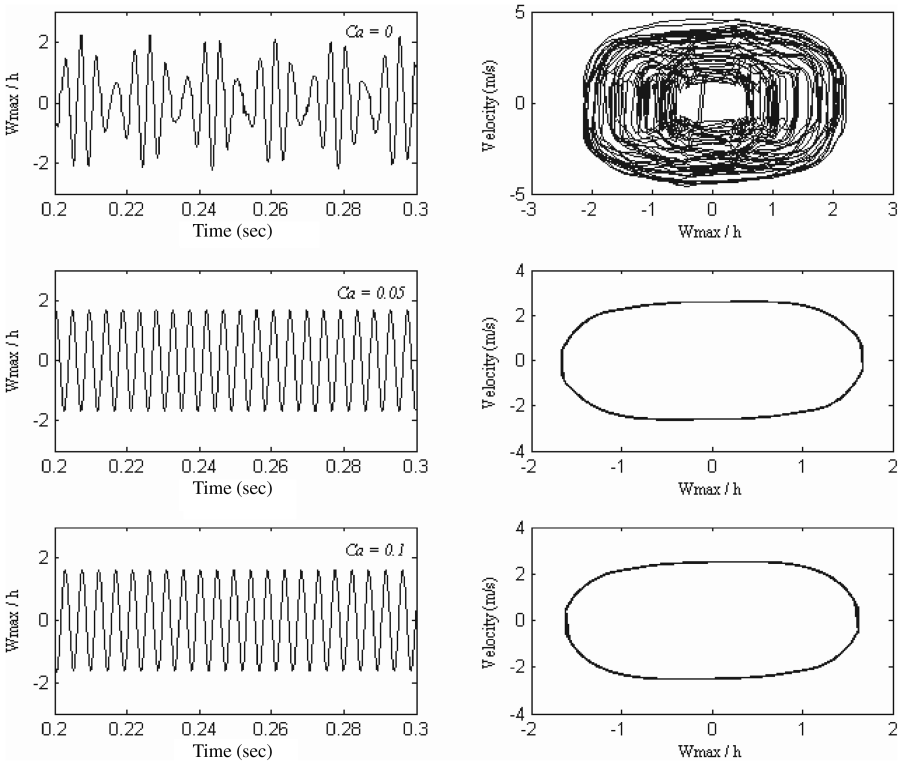

Fig. 6 Effect of aerodynamic damping coefficient *Ca* on the flutter behavior of a simply supported composite panel at $\lambda = 700$.

shows nearly harmonic limit-cycle oscillations as depicted in the phase plots. In addition, a very small change in the amplitude is found by raising the damping value up to 0.1.

Time history responses and phase plots of the composite panel at $\lambda = 0$, SPL = 110 dB, and temperature rises $\Delta T = 0$, 50, 100, and 150°C are presented in Figs. 7 and 8. At room temperature, the panel is seen to randomly vibrate with deflections rms = 0.727. For $\Delta T = 50$°C, which is beyond the critical buckling temperature ΔT_{cr} of this panel [22], the nonlinear stiffness added to the panel due to thermal postbuckling deflection led to small amplitude vibrations about one of the postbuckling equilibrium deflections. Moreover, the panel shows intermittent snap-through motions between the two thermal buckling equilibrium positions. Occurrence of the snap-through motion is resisted by the nonlinear stiffness added to the panel due to the increased thermal deflection at $\Delta T = 100$°C, resulting in smaller number of snap-through motions. At $\Delta T =$ 150°C, the snap-through motion is seen to be completely hindered, and the plate shows smaller vibration amplitudes about one of the thermal buckling equilibrium positions. Because the SMAHC panel remains flat up to a temperature rise of $\Delta T = 100$°C, it can be observed in Fig. 9 that the panel exhibits moderate deflection random vibration for the temperature rises while having higher vibration amplitudes at $\Delta T = 50$ and 100°C than those of the composite panel. At a temperature rise of 150°C, which is beyond the critical buckling temperature of the SMAHC panel [22], it is seen that the panel experiences a persistent snap-through which covers both thermal

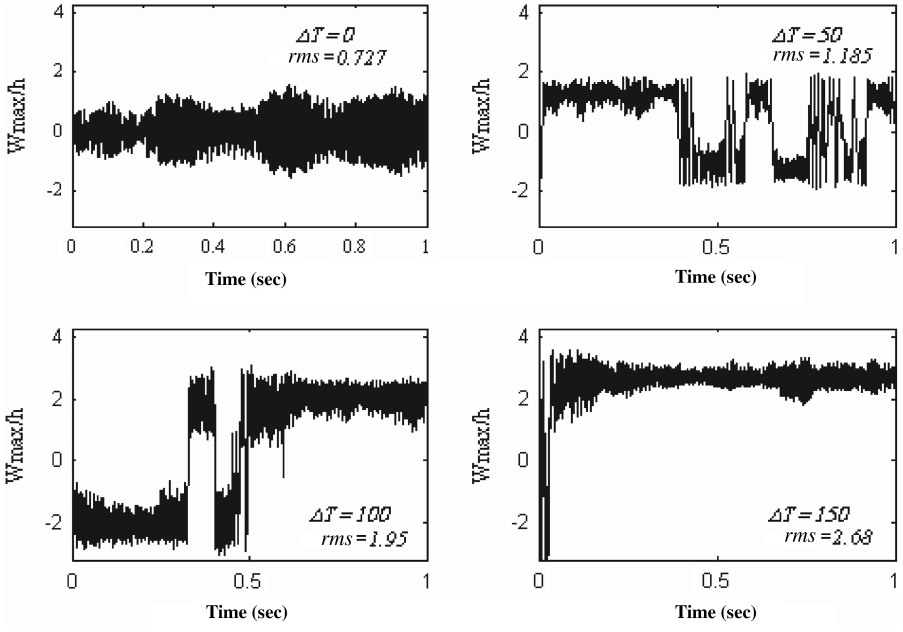

Fig. 7 Time history response of the composite panel at SPL = 110 dB, $\lambda = 0$, and at different temperature rises ΔT.

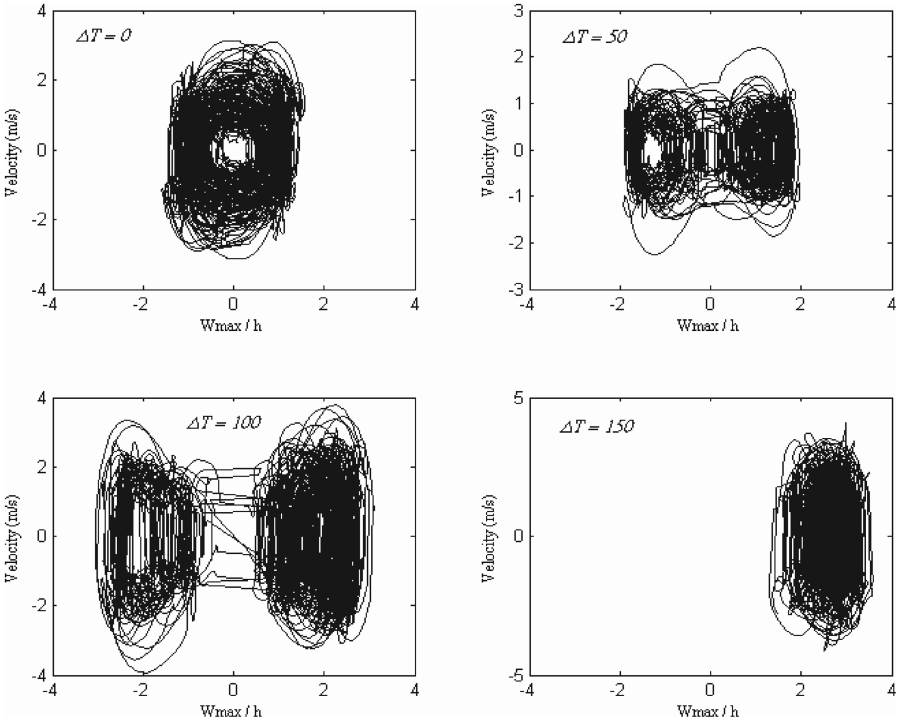

Fig. 8 Phase plots of the composite panel at SPL = 110 dB, λ = 0, and at different temperature rises ΔT.

buckling equilibrium positions because the nonlinear stiffness has not yet compensated the critically lowered stiffness due temperature rise. It is also observed that the SMAHC panel has almost the same rms deflections at $\Delta T = 50$ and 100°C, because the SMA recovery stresses compensate the adverse effect of the thermal stresses in this temperature range. Therefore, it becomes a matter of compromise between having a thermally buckled panel with smaller vibration amplitudes, which affects the aerodynamic performance, and having a flat panel with higher vibration amplitudes, which affects the fatigue life performance of the panel.

To study the effect of having an airflow along with a random acoustic pressure, Fig. 10 illustrates the nonlinear vibration behavior of a composite panel with $\lambda = 400$ and SPL = 110 dB. At room temperature, the presence of airflow is found to have a noticeable effect on the composite panel stiffness through highly decreasing the deflection rms value compared with the $\lambda = 0$ case presented in Fig. 7. At a temperature rise value of 50°C, the $\lambda = 400$ value exceeds the critical flutter value. Therefore, the panel shows nearly harmonic limit-cycle oscillations which totally dominate the acoustic random excitation. Because of the interaction between the aerodynamic flow and the nonlinear stiffness added to the plate due to the higher thermal postbuckling deflections at $\Delta T = 100$ and 150°C, the panel is seen to have chaotic limit-cycle oscillations which can add complexity to the fatigue life analysis. For the SMAHC panel presented in Fig. 11, the tension field generated by the constrained shape recovery process of the SMA fiber embeddings compensate the reduced stiffness of the panel due to thermal stresses at $\Delta T = 50$ and 100°C, resulting in a critical flutter value higher than the $\lambda = 400$

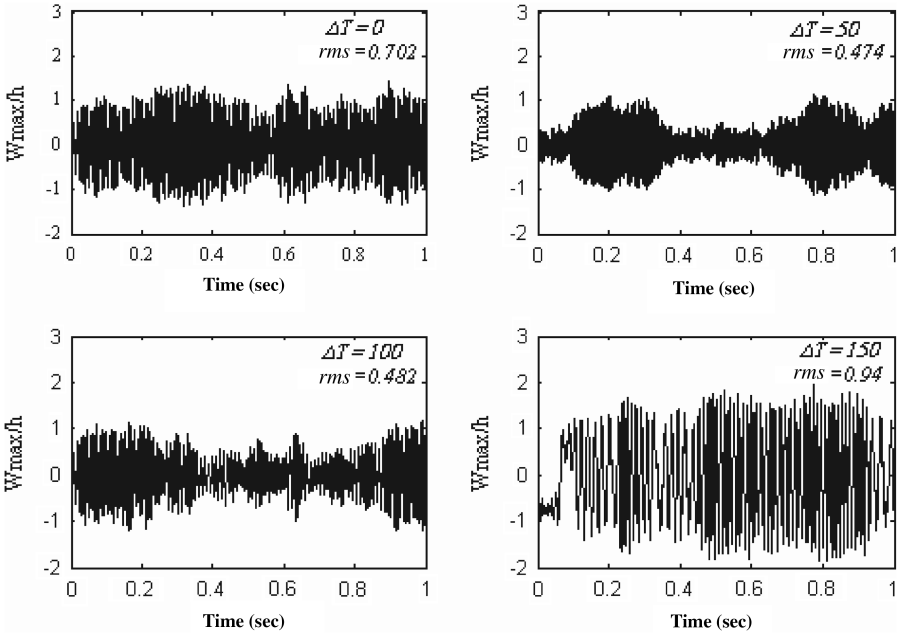

Fig. 9 Time history response of the SMAHC panel at SPL = 110 dB, λ = 0, and at different temperature rises ΔT.

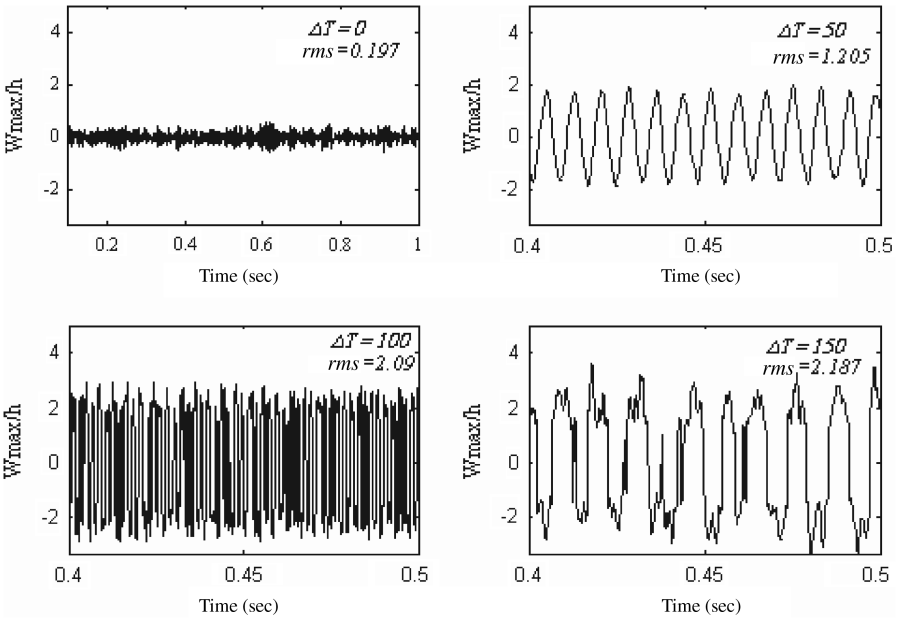

Fig. 10 Time history response of the composite panel at SPL = 110 dB, λ = 400, and at different temperature rises ΔT.

value. Therefore, the airflow is found to add more stiffness to the panel, resulting in very small vibration amplitudes at these temperatures compared to the flutter motion illustrated in Fig. 10. In addition, due to the low panel stiffness in the vicinity of the critical buckling temperature rise, the SMAHC panel is seen to have higher deflection rms at $\Delta T = 150$°C than that of $\Delta T = 100$°C.

At room temperature, increasing the value of λ up to 700 is found not to add more stiffness to the composite panel shown Fig. 12, because the critical nondimensional dynamic pressure value has been exceeded and the panel experiences flutter instability. But, the interaction between acoustic pressure and the flutter motion lead to a chaotic response with a lower deflection rms than that of Fig. 7. At higher temperatures, the aerodynamic instability is seen to dominate the response showing near values of the flutter limit-cycle oscillation amplitudes, whereas the vibration becomes more chaotic with increasing temperature due to the interaction of the nonlinear stiffness added by the increased thermal postbuckling deflection. For the SMAHC panel presented in Fig. 13, no noticeable change is found at room temperature compared to the composite panel as the SMA fibers are not activated yet. But at higher temperatures, a pronounced enhancement in the response is found through having very small deflection rms values compared with those of the composite panel presented in Fig. 12.

The effect of increasing the SPL from 110 up to 130 dB at λ = 700 is presented in Figs. 14 and 15. At room temperature, it is seen in Fig. 14 that the value of the deflection rms of the composite panel increased from 0.548 up to 1.2 by increasing the sound pressure. At higher temperatures, it is found that the random acoustic response completely dominates the flutter motion, resulting in a much lower deflection rms values than those of Fig. 12. Moreover, the panel shows a persistent snap-through motion which covers both buckling equilibrium positions, because the higher acoustic pressure can overcome the nonlinear stiffness added to the panel by thermal deflections. Although, the SMAHC panel presented in Fig. 15 still shows a better performance through having a lower deflection rms values compared to those of the composite panel.

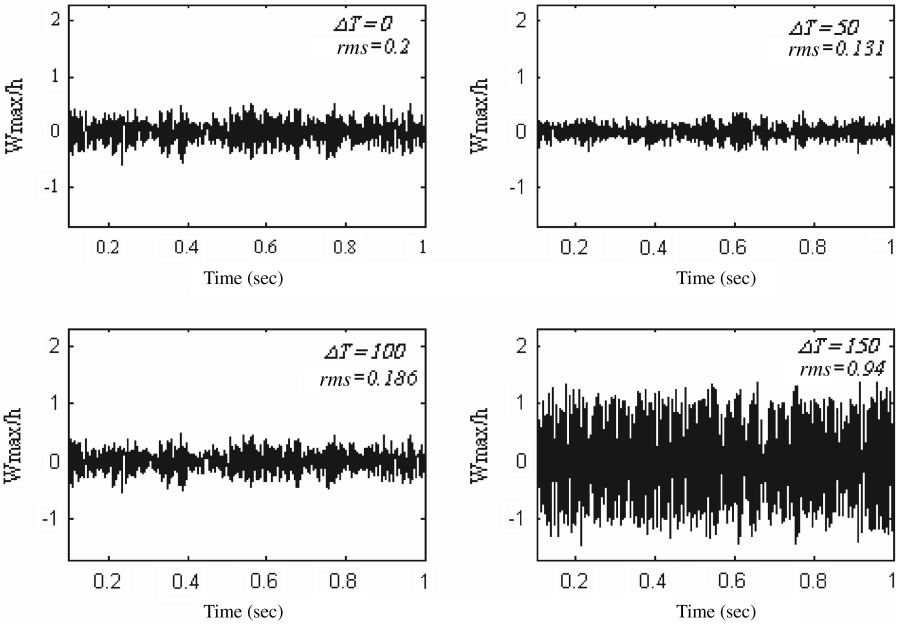

Fig. 11 Time history response of the SMAHC panel at SPL = 110 dB, λ = 400, and at different temperature rises ΔT.

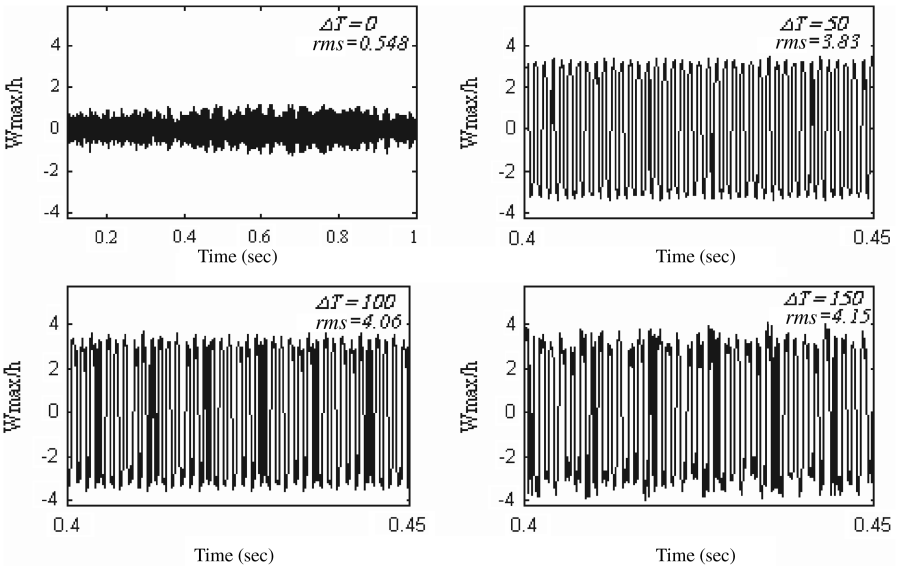

Fig. 12 Time history response of the composite panel at SPL = 110 dB, λ = 700, and at different temperature rises ΔT.

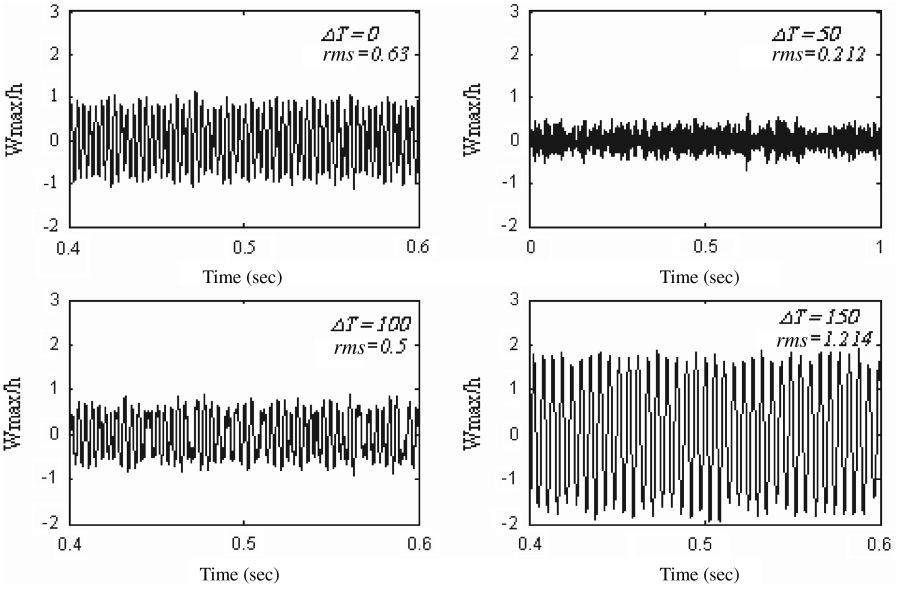

Fig. 13 Time history response of the SMAHC panel at SPL = 110 dB, λ = 700, and at different temperature rises ΔT.

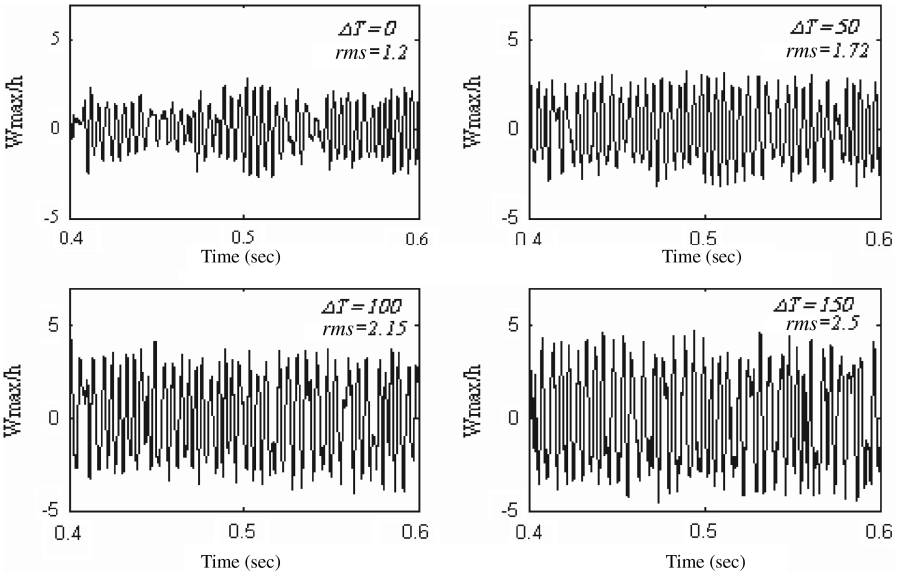

Fig. 14 Time history response of the composite panel at SPL = 130 dB, λ = 700, and at different temperature rises ΔT.

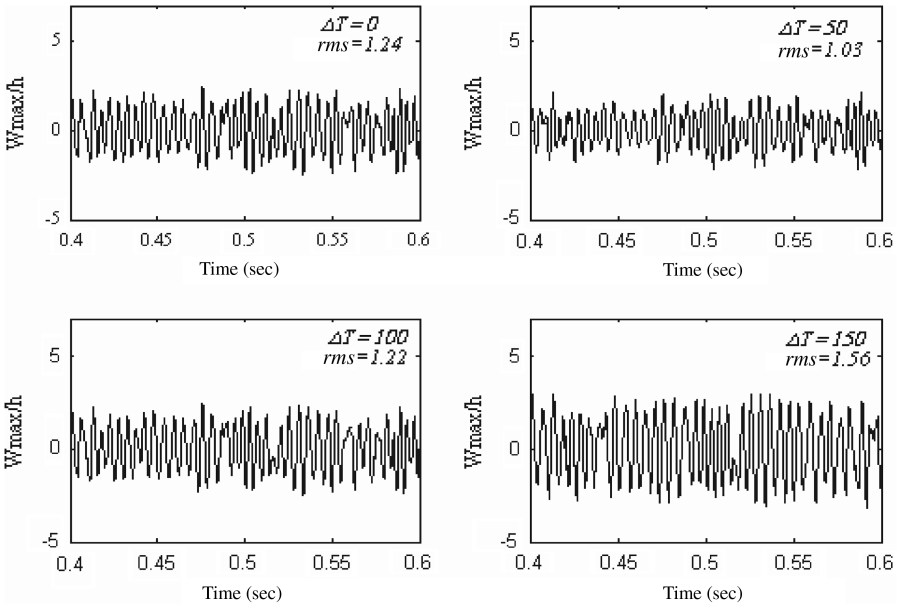

Fig. 15 Time history response of the SMAHC panel at SPL = 130 dB, λ = 700, and at different temperature rises ΔT.

V. Conclusions

A time-domain solution was presented for the supersonic nonlinear vibration behavior of clamped SMAHC panels under combined aerodynamic, thermal, and random acoustic loads. A nonlinear finite element model was provided based on the first-order shear plate theory with von Kármán geometric nonlinearity and the principle of virtual work. The constrained shape recovery feature of SMA fibers is used to control the dynamic response of composite panels at elevated temperatures. Nonlinear temperature-dependence of material properties was considered in the formulation. Newton–Raphson iteration is employed to obtain the dynamic response at each time step of the Newmark numerical integration scheme. A solution procedure using modal transformation is developed for the time-domain method.

It is concluded that studying the interaction of the acoustic pressure and the aerodynamic flow at elevated temperatures is very important, whereas overlooking their simultaneous action can affect the accuracy of fatigue life determination. Results also demonstrated the importance of SMA fiber embeddings in controlling the dynamic response at elevated temperatures and high random acoustic excitations through postponing the occurrence of flutter along with decreasing the vibration amplitudes. However, at certain loading conditions, it turns out to be a matter of compromise between having a thermally buckled composite panel with smaller vibration amplitudes, which affects the aerodynamic performance, and having a flat SMAHC panel with higher vibration amplitudes, which affects the fatigue life performance of the panel.

References

[1] Dowell, E. H., "A Review of the Aeroelastic Stability of Plates and Shells," *AIAA Journal*, Vol. 8, No. 3, 1970, pp. 385–399. doi:10.2514/3.5680

[2] Mei, C., Abdel-Motagaly, K., and Chen, R., "Review of Nonlinear Panel Flutter at Supersonic and Hypersonic Speeds," *Applied Mechanics Reviews*, Vol. 52, No. 10, 1999, pp. 321–332. doi:10.1115/1.3098919

[3] Dixon, I. R., and Mei, C., "Finite Element Analysis of Large-Amplitude Panel Flutter of Thin Laminates," *AIAA Journal*, Vol. 31, No. 4, 1993, pp. 701–707. doi:10.2514/3.11606

[4] Xue, D. Y., and Mei, C., "Finite Element Nonlinear Panel Flutter With Arbitrary Temperatures in Supersonic Flow," *AIAA Journal*, Vol. 31, No. 1, 1993, pp. 154–162. doi:10.2514/3.11332

[5] Liaw, D. G., "Nonlinear Supersonic Flutter of Laminated Composite Plates Under Thermal Loads," *Computers and Structures*, Vol. 65, No. 5, 1997, pp. 733–740. doi:10.1016/S0045-7949(94)00487-0

[6] Abdel-Motagaly, K., Chen, R., and Mei, C., "Effects of Flow Angularity on Nonlinear Supersonic Flutter of Composite Panels Using Finite Element Method,"AIAA, Reston, VA, 1999, pp. 1963–1972.

[7] Vaicaitis, R., "Nonlinear Response and Sonic Fatigue of National Aerospace Space Plane Surface Panels," *Journal of Aircraft*, Vol. 31, No. 1, 1994, pp. 10–18. doi:10.2514/3.46449

[8] Istenes, R. R., Rizzi, S. A., and Wolfe, H. F., "Experimental Nonlinear Random Vibration Results of Thermally Buckled Composite Panels,"AIAA, Washington, D.C., April 1995, pp. 1559–1568.

[9] Ng, C. F., and Clevenson, S. A., "High-Intensity Acoustic Tests of a Thermally Stressed Plate," *Journal of Aircraft*, Vol. 28, No. 4, 1991, pp. 275–281. doi:10.2514/3.46023

[10] Murphy, K. D., Virgin, L. N., and Rizzi, S. A., "Characterizing the Dynamic Response of a Thermally Loaded Acoustically Excited Plate," *Journal of Sound and Vibration*, Vol. 196, No. 5, 1996, pp. 635–658. doi:10.1006/jsvi.1996.0506

[11] Kavallieratos, P., and Vaicaitis, R., "Nonlinear Response of Composite Panels of High Speed Aircraft," *Composites Engineering*, Vol. 3, Nos. 7–8, 1993, pp. 645–660. doi:10.1016/0961-9526(93)90088-2

[12] Locke, J. E., "Finite Element Large Deflection Random Response of Thermally Buckled Plates," *Journal of Sound and Vibration*, Vol. 160, No. 2, 1993, pp. 301–312. doi:10.1006/jsvi.1993.1025

[13] Abdel-Motagaly, K., Duan, B., and Mei, C., "Nonlinear Response of Composite Panels Under Combined Acoustic Excitation and Aerodynamic Pressure," *AIAA Journal*, Vol. 38, No. 9, 2000, pp. 1534–1542. doi:10.2514/2.1175

[14] Dhainaut, J. M., Guo, X., and Mei, C., "Nonlinear Random Response of Panels in an Elevated Thermal-Acoustic Environment," *Journal of Aircraft*, Vol. 40, No. 4, 2003, pp. 683–691. doi:10.2514/2.3146

[15] Birman, V., "Review of Mechanics of Shape Memory Alloy Structures," *Applied Mechanics Reviews*, Vol. 50, No. 11, 1997, pp. 629–645. doi:10.1115/1.3101674

[16] Jia, J., and Rogers, C. A., "Formulation of a Mechanical Model for Composites with Embedded SMA Actuators," *Journal of Mechanical Design*, Vol. 114, No. 4, 1992, pp. 670–676. doi:10.1115/1.2917059

[17] Tawfik, M., Ro, J. J., and Mei, C., "Thermal Post-Buckling and Aeroelastic Behavior of Shape Memory Alloy Reinforced Plates," *Smart Materials and Structures*, Vol. 11, No. 2, 2002, pp. 297–307. doi:10.1088/0964-1726/11/2/313

[18] Park, J. S., Kim, J. H., and Moon, S. H., "Vibration of Thermally Post-Buckled Composite Plates Embedded with Shape Memory Alloy Fibers," *Composite Structures*, Vol. 63, No. 2, 2004, pp. 179–188.

doi:10.1016/S0263-8223(03)00146-6

[19] Gilat, R., and Aboudi, J., "Dynamic Response of Active Composite Plates: Shape Memory Alloy Fibers in Polymeric/Metallic Matrices," *International Journal of Solids and Structures*, Vol. 41, No. 20, 2004, pp. 5717–5731. doi:10.1016/j.ijsolstr.2004.04.043

[20] Ibrahim, H. H., Tawfik, M., and Negm, H. M., "Thermal Post-Buckling and Flutter Behavior of Shape Memory Alloy Hybrid Composite Plates," American Society of Mechanical Engineers Paper ICFDP-EG-153, Dec. 2006.

[21] Guo, X., Lee, Y. Y., and Mei, C., "Supersonic Nonlinear Panel Flutter Suppression Using Shape Memory Alloys," *Journal of Aircraft*, Vol. 44, No. 4, 2007, pp. 1139–1149. doi:10.2514/1.16080

[22] Ibrahim, H. H., Tawfik, M., and Negm, H. M., "Random Response of Shape Memory Alloy Hybrid Composite Plates Subject to Thermo-Acoustic Loads," *Journal of Aircraft*, Vol. 45, No. 3, 2008, pp. 962–970. doi:10.2514/1.32843

[23] Reddy, J. N., *Theory and Analysis of Elastic Plates*, Taylor and Francis, London, 1999.

[24] Xue, D. Y., "Finite Element Frequency Domain Solution of Nonlinear Panel Flutter with Temperature Effects and Fatigue Life Analysis," Ph.D. Dissertation, Mechanical Engineering Dept., Old Dominion Univ., Norfolk, Virginia, 1991.

[25] Bathe, K. J., *Finite Element Procedures*, Prentice–Hall, Englewood Cliffs, NJ, 1996.

[26] Yoo, H. H., "Dynamic Modelling of Flexible Bodies in Multibody Systems," Ph.D. Dissertation, Mechanical Engineering Dept., Univ. of Michigan, Dearborn, MI, 1989.

[27] Cross, W. B., Kariotis, A. H., and Stimeler, F. J., "Nitinol Characterization Study," NASA CR-14B, 1969.

[28] Stearns, S., and David, R., *Signal Processing Algorithms in Matlab*, Prentice–Hall, Series Editor Allan V. Oppenheim, Upper Saddle River, NJ, 1996.

[29] Dowell, E. H., "Nonlinear Oscillation of a Fluttering Plate I," *AIAA Journal*, Vol. 4, No. 7, 1966, pp. 1267–1275. doi:10.2514/3.3658